Physicochemical Characterization of Chitosan-Multiwalled Carbon Nanotubes Hybrid Material for Ofloxacin Delivery

Zainab Jasim Khudair[1*] and Zeina Mohammad Kadam[2]

[1]*Department of Science, College of Basic Education, Al-Muthanna University, Al-Qishla, Samawah 66001, Iraq*

[2]*Department of Chemistry, College of Science, Al-Qadisiyah University, Um-Alkhail, Diwaniyah 58001, Iraq*

* ***Corresponding author:***

email: chemistry.zainb@mu.edu.iq

Received: June 15, 2024
Accepted: August 3, 2024

DOI: 10.22146/ijc.97160

Abstract: *The present study involved the synthesis of a bioactive composite material using chitosan (CS) and multi-walled carbon nanotubes (MWCNTs) through the free radical polymerization method. The resulting composite material was comprehensively characterized using various experimental techniques, such as Fourier-transform infrared spectroscopy (FTIR) and X-ray diffraction (XRD). The quantification of the swelling behavior involved the measurement of changes in the weight of the sample as a function of the time it was immersed in an aqueous buffered solution. The findings indicated that the maximum drug-loading rate of ofloxacin medication (OFL) was 86%. Moreover, the pH sensitivity of the poly acrylic acid grafting multi-walled carbon nanotubes p(CS-co-AA)/MWCNTs nanocomposite facilitated the substantial release of a significant quantity of medication in aqueous buffered solution at a pH of 1.2. The average rate of drug release was measured to be 76% after 72 h duration. On the other hand, the release of the drug at pH 5 and 7.4 was 42% and 32%, respectively. According to the reported findings, the p(CS-co-AA)/MWCNTs carrier has a favorable capacity to control the release of the OFL drug into the intended medium while reducing potential negative effects.*

Keywords: *MWCNT; ofloxacin drug; drug loading; swelling ratio;* in vitro *release*

■ INTRODUCTION

In recent years, nanotechnology has emerged as a significant technology that can enhance the quality of life and promote the well-being of society. As a result, various government agencies provide increased financial support for different research studies on nanomaterials [1]. Nanotechnology encompasses examining and controlling materials at the atomic and molecular scale. Several novel formulations have been developed to improve the effectiveness of therapy and reduce undesirable adverse reactions, as demonstrated by *in vitro* and *in vivo* studies [2].

Researchers have recently evaluated different nano-sized drug delivery vehicles, such as nanotubes, which are synthetic materials made up of carbon atoms [3]. Various nanotubes are available, including short, long, open, closed, single-walled, double-walled, multi-walled, and spiral structures. Nanotubes are built based on their length-to-diameter ratio, which can be as large as 132,000,000:1. These cylindrical carbon molecules with hollow interiors have unique characteristics that render them valuable for numerous applications such as optics, electronics, biomedical, nanotechnology, and other fields of material science [4-8].

Carbon nanotubes (CNTs) exhibit limited solubility in both aqueous and organic mediums due to their tendency to agglomerate. This characteristic has posed significant challenges in biomedical and biological applications. Recent efforts have focused on functionalizing CNTs by modifying their chemical structure to address this issue. This modification enhances their dispersion and solubility in various mediums [9-13]. Covalent modification involves modifying CNTs directly through sidewall functionalization, which offers benefits such as high solubility, low toxicity, and the ability to alter the structure and load drugs. Non-covalent modification

involves wrapping biopolymers, surfactants, and polymers to achieve high solubility, low toxicity, moderate degradation capacity, and high drug loading and structural alterations [14].

Using CNTs in drug delivery systems offers many processes, such as adsorption and covalent binding, which can be selected based on the specific requirements of the system being created. This versatility is attributed to the abundant surface chemistry exhibited by CNTs [15-16].

Since the adsorption/desorption mechanism does not require any modification of the drug molecule's chemical structure, unlike covalent binding, it raises fewer concerns about the drug's bioactivity. It can be used to design smart, environment- and stimuli-responsive CNTs drug delivery and release systems with relative simplicity and broad applicability [17-19]. The affinity between chemotherapeutic drugs and CNTs, the thermodynamics and kinetics of adsorption, the influence of pH, ionic composition, CNTs purity, dispersion state, surface chemistry, and other essential factors are crucial considerations in the development of practical CNT-based systems for delivering anticancer drugs or other medications such as antibiotics. These parameters also play a critical role in ensuring safe and effective drug delivery, minimizing side effects and toxicity associated with conventional treatments like oral and injection medicines [20]. In specific circumstances, it may be viable to provide higher doses of a drug to alleviate the symptoms of the illness [21]. Recent research indicates that nanotechnology plays a substantial role in serving as a carrier for drug delivery [22] and enables control over time and location of drug release within the body [23-24]. One of the key advantages of drug delivery systems is their ability to administer a substantial quantity of drug molecules while minimizing the occurrence of severe side effects, all without inducing toxicity [25].

The distribution of topical ophthalmic solutions is greatly affected by the quick turnover and drainage of tear fluid, leading to substantial loss of medication in the precorneal region. According to certain sources, it has been proposed that only 5% of the prescribed dose effectively enters the eye through injection. Simultaneously, it is assumed that the remaining fraction is absorbed systemically by the conjunctiva and nasolacrimal duct. Recent research in ophthalmic drug delivery systems has prioritized enhancing many factors, such as prolonging the contact period of the vehicle with the ocular surface, delaying the outflow of medication, and enhancing corneal absorption [26-27]. Chitosan (CS) is a highly significant film polymer, ranking second to cellulose polymers. Its exceptional functional and biological characteristics make it well-suited for research and applications in pharmaceuticals and biomedicines [28].

Ofloxacin (OFL) is categorized as a fluoroquinolone antibacterial antibiotic. This medicine is used to treat infections that affect the urinary and respiratory systems, as well as illnesses such as gonorrhea and dermatological ailments. The optimal dosage for this infection may vary based on its severity, ranging from 200 to 600 mg, with a frequency of administration of 2 to 3 times daily. Under more extreme conditions, it can be imperative to prolong the duration of the treatment. The medication demonstrates a biological half-life ranging from 5 to 6 h [29]. The goal of this study is to prepare new pH-sensitive gelatinous polymeric nanocomposites, designed based on cross-linked polymers containing natural pharmaceutical polymers such as CS, to develop controlled drug delivery systems. This includes formulating a gastroretentive sustained drug release system for OFL medication, which aims to improve their retention time, pharmacological activity, bioavailability, and therapeutic efficacy.

■ EXPERIMENTAL SECTION

Materials

All starting materials and solvents that were used in the synthesis of the target compounds were supplied from available sources and were directly used without further purification. Multi-walled carbon nanotubes (MWCNTs) powder (5 g, outer diameter (OD) = 40–60 nm, 5–10 μm, 99.0% purity, surface area > 200 m^2/g, layers = 7, density = 2.1 g/cm^3) was obtained from VCN Materials, Co., Ltd, Iran. CS (medium molecular weight, 96%) was purchased from HIMEDIA. MACLIN from

China provides OFL. Acrylic acid was purchased from Merck, Germany. Acetic acid 99.5% and *N,N'*-methylenebisacrylamide (MBA, 99.0%) as cross-linkers were purchased from CDH, India. The initiator is potassium persulfate (KPS, 99.0%), supplied by Thomas Baker, India. Calcium chloride, sodium chloride, sodium hydroxide, potassium chloride, and hydrochloric acid were supplied from Fluka, Germany. All solutions were prepared by using deionized water (DI).

Instrumentation

FTIR spectra were registered to the surface before and after loaded ofloxacin with a Bruker, Germany (model: Equinox 55, Tensor 27), KBr at a range of 400–4000 cm^{-1}. XRD was collected from a Philips, USA diffractometer (model: PW1730). Field emission scanning electron microscopy (FESEM) indicated the microscopic study of the products with a Tescan instrument, Czech Republic (model: Mira3), and transmission electron microscope (TEM) via Philips, Nederland (model: EM208S). Thermogravimetric analysis (TGA/DSC) was determined by TA Instruments, USA (model: Q600). Nitrogen adsorption-desorption isotherms were indicated by the BET device of the BEL, Japan (Model: Belsorp mini II). Zeta potential was determined on a Malvern Instrument Zetasizer Nano-ZS at room temperature. EDX is the same as the FESEM device, only detector changes (SE).

Procedure

Preparation of poly(CS-co-AA)/MWCNTs nanocomposite

An amount of 0.5 g of CS (MW = 3800–20000 Daltons, De. > 75%) was dispersed in 20 mL of 1% aqueous acetic acid to prepare a 2.5 wt.% of CS solution. The mixture was stirred for 15 min to complete the dispersal of CS polymer. Then, 10 mL of MWCNTs solution (1 mg/mL in DI.W) was treated under a probe sonication (650 Watts) for 10 min and added to the CS solution. During this step, CS macromolecules were adsorbed on the surface of the MWCNTs, thereby acting as polymer cationic surfactants that stabilize the MWCNTs [30].

A weight of 0.02 g in 2.00 mL DI.W of the initiator KPS was added to the previous solution, along with 15.00 mL of acrylic acid, which acts as a monomer, then the cross-linker (0.02 g in 2 mL DI.W MBA), while still stirring at 65 °C, was added to the mixture. The mixture was bubbled with nitrogen gas for 1 min to get rid of oxygen, poured into tubes and put in a water bath at 70 °C for 2 h to complete the polymerization process. The resulting nanocomposite was sectioned into similar

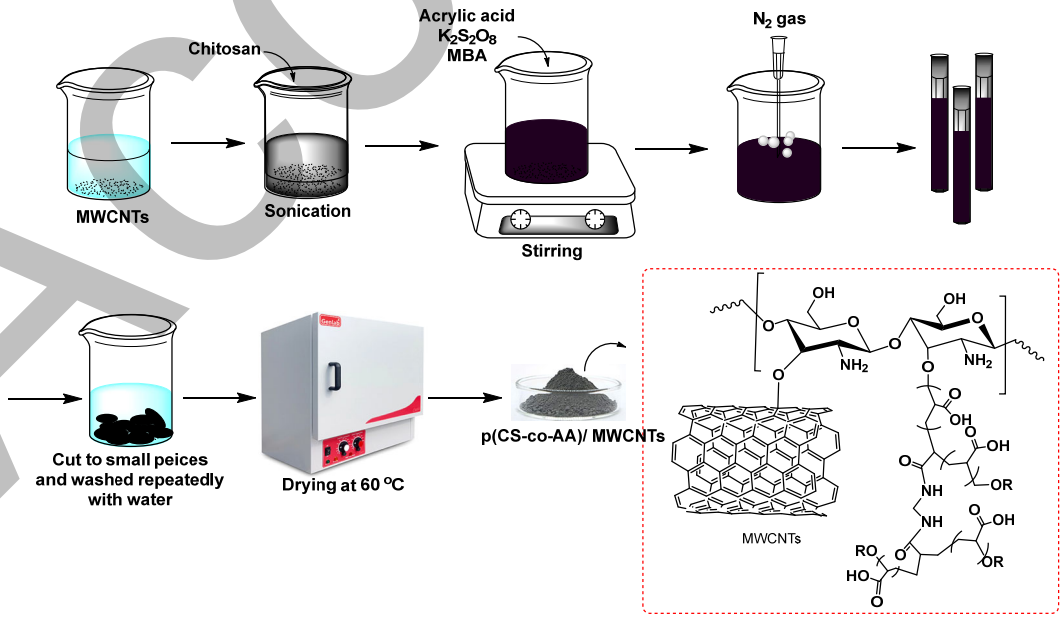

Fig 1. Graphical synthetic route of p(CS-co-AA)/MWCNTs

pieces (thickness ≈5 mm) and then washed several times with DI.W for 24 h, which it replaced with fresh DI.W repeatedly to remove all the unreacted monomers. After washing the nanocomposite, it was dried at 60 °C in a dryer oven to constant weight. Finally, the dried p(CS-co-AA)/MWCNTs were ground, sieved (T77 type sieve with 28 μm diameter), and stored in airtight containers for further use [31], Fig. 1 shows the synthetic route of p(CS-co-AA)/MWCNTs.

Swelling studies

The tea-bag method is widely recognized as the traditional approach for analyzing limited quantities of samples [32-34]. p(CS-co-AA)/MWCNTs nanocomposite powders with initial weight W_0 from 0.01 to 0.03 g were packed in already-weighed tea bags and hung in the beakers containing an excessive amount of various buffers ranging from pH 2 to 10 at room temperature for a designated duration of time t (about 20 h). Subsequently, the tea bags from each buffer solution were periodically extracted, placed onto a dry towel, and delicately cleaned using another dry cloth to eliminate any surplus liquid and loosely bound moisture. The tea bags were then weighed. The weight of the tea bag is subsequently measured as W_2. The same procedure is similarly carried out for an empty bag, and the weight of the bag is measured as W_1. The swelling percentage at time t is determined using Eq. (1).

$$\text{Swelling } (\%) = \frac{W_2 - W_1 - W_0}{W_0} \times 100\% \quad (1)$$

Water evaporation rate

The water retention capacity of p(CS-co-AA)/MWCNTs nanocomposite in water was evaluated by placing the fully hydrated samples at 25 °C for the setting duration, the water evaporation ratio was determined by measuring the initial weight (W_1), measured weight (W_2) and the final weight (W_3) of the nanocomposite and continuously monitoring the weight, this process is continued until no change in weight [35], according to Eq. (2).

$$\text{Water lost } (\%) = \frac{W_1 - W_2}{W_1 - W_3} \times 100\% \quad (2)$$

Drug loading and drug release behavior

A stock solution of OFL at a concentration of 500 mg/L was prepared using distilled water, and the maximum wavelength of the solution was recorded. A volume of 100 mL of the OFL solution was taken from the stock solution. A quantity of 50 mg of the nanocomposite was introduced into a flask containing OFL solution. The mixture was subjected to stirring for 2 h, followed by an incubation period of 24 h [36]. The spectrophotometric monitoring of the loading efficacy of OFL in the nanocomposite sample was performed. The sample was then filtered and dried at 50 °C, and the drug loading result was calculated using Eq. (3).

$$\text{Drug loading } (\%) = \frac{\text{weight of drug in sample}}{\text{weight of sample taken}} \times 100\% \quad (3)$$

To study drug release, 50 mg of p(CS-co-AA)/MWCNTs OFL-loaded were placed in dialysis bags and immersed in buffer solutions with pH values of 1.2, 5.0, and 7.4. The test was conducted in a shaking incubator at 37 °C [37]. Concentrations of the drug released were determined at several time intervals (0–72 h) and at different pH conditions (1.2, 5.0, and 7.4). Throughout the incubation process, a 3.0 mL portion of the sample was extracted from the solution at regular intervals and substituted with an equal quantity of buffer solution to ensure a consistent volume of the release medium. The quantity of OFL produced from the nanocomposite was examined by quantifying the intensity of UV absorbance at 272 nm using a UV–vis spectrophotometer. The cumulative release of OFL was determined by applying Eq. (4) [38];

$$\text{Cumulative release } (\%) = \left[C_n + \frac{3}{10} \sum C_{n-1} \right] \times 100\% \quad (4)$$

where C_n and C_{n-1} are the amount of drug released at the time n and n–1, respectively.

■ RESULTS AND DISCUSSION

Characterization of *p*(CS-*co*-AA)/MWCNTs Nanocomposite Before and After OFL Loaded

FTIR spectra of the p(CS-co-AA)/MWCNTs nanocomposite before and after OFL loaded are indicated in Fig. 2(a) and 2(b). The spectra are comparable each other due to the similarities in their structures, with the exception of the OFL drug's characteristic C–F band at 1253 cm^{-1}.

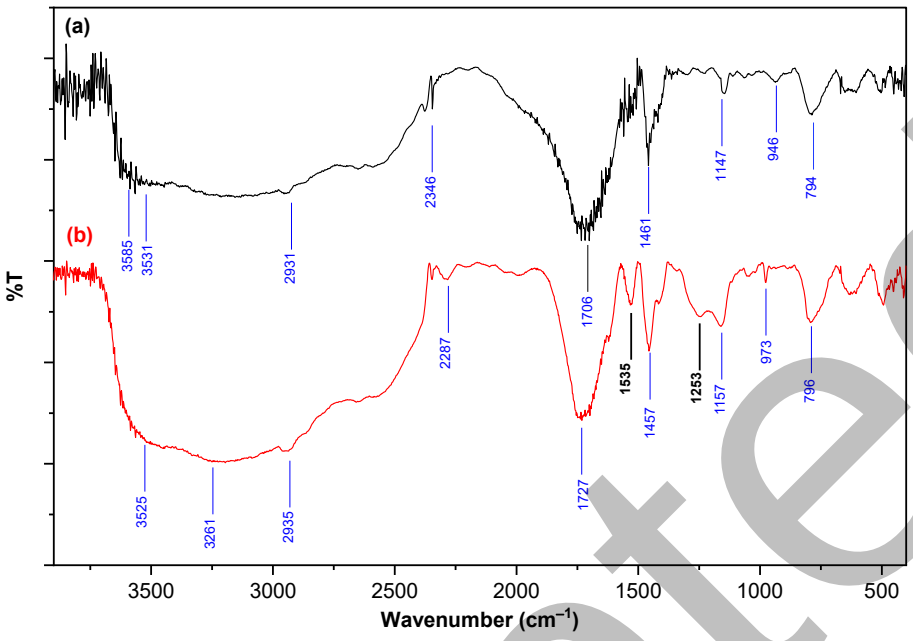

Fig 2. FTIR spectra of p(CS-co-AA)/MWCNTs (a) before and (b) after OFL loaded

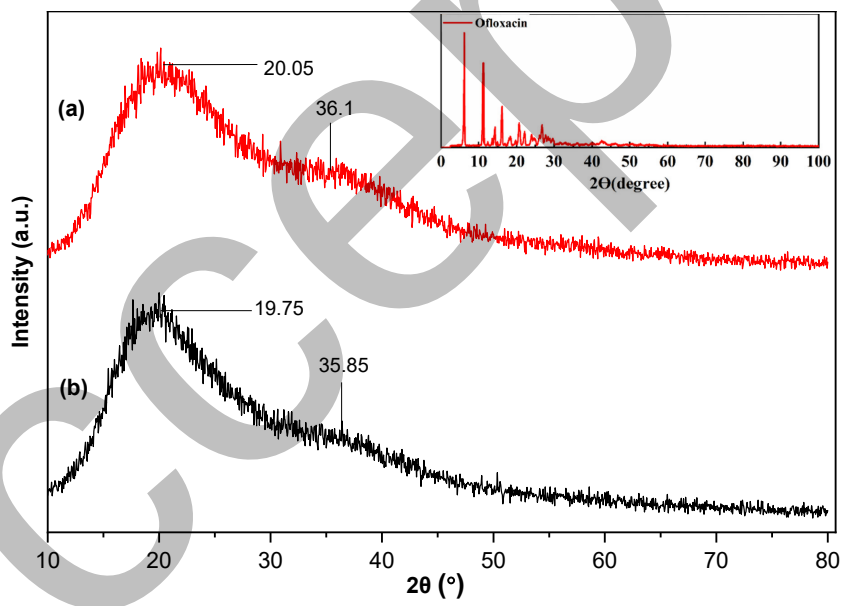

Fig 3. XRD patterns of (a) p(CS-co-AA)/MWCNTs before and (b) after OFL loaded (inset XRD for OFL)

The spectra also indicate the presence of peaks in 1147 and 1157 cm^{-1} of the C–O group in CS for both composites. The appearance of peaks at 1706 and 1727 cm^{-1} illustrates the C=O of the acrylic acid, and the adsorption bands at 2931 and 2935 cm^{-1} indicate the C–H aliphatic group in acrylic acid. The prominent band observed in the spectrum, from around 2500 to 3500 cm^{-1}, can be attributed to the hydrogen bonding in both composites.

Fig. 3 presents the XRD patterns of the p(CS-co-AA)/MWCNTs nanocomposite before and after loading with OFL. The absence of distinct diffraction patterns implies that the samples possess an amorphous structure. Only a broad diffraction band at a 2θ angle of 20 was observed, characteristic of amorphous CS composites. Moreover, the presence of polyacrylic acid in this composite is evidenced by the peaks at position 36. This finding aligns with the observation in the previous study

[39] for amorphous CS composite. There was no phase change in the immobilization of OFL drug onto p(CS-co-AA)/MWCNTs.

Fig. 4 displays the FESEM images of the p(CS-co-AA)/MWCNTs (4(a),4(b)) and OFL (4(c),4(d)). The composites are both rough, non-smooth and uneven in texture. p(CS-co-AA)/MWCNTs have a rougher surface than OFL, which enhances the specific surface area. The low surface area can be related to the adsorption of the drug molecules onto the surface, resulting in the block of many pores and thereby rendering the surface visually smoother. Additionally, porosity can be observed on the surface of the p(CS-co-AA)/MWCNTs, leading to enhanced adsorbent characteristics. Another factor that may be observed in the FESEM is the appropriate distribution of the drug within the adsorbent structure.

Fig. 5(a)-5(d) displays TEM images of composites consisting of p(CS-co-AA)/MWCNTs and OFL. The composite TEM images revealed the absence of distinguishable MWCNTs, suggesting a high level of uniformity and a substantial influence of CS on CNTs. Fig. 5(a) and 5(b) display a porous and hollow structure with irregularly shaped particles. Aligned pores are clearly apparent, showing the presence of a porous architecture. This porous structure contributes to the large specific surface area of p(CS-co-AA)/MWCNTs. The TEM micrograph of the OFL composite is shown in Fig. 5(c) and 5(d) and numerous pores are enclosed by OFL molecules. The drug acts as a blinder material, increasing the degree of aggregation that occurs upon loading. Both FESEM and TEM micrographs agree with BET studies regarding the specific surface area and pore

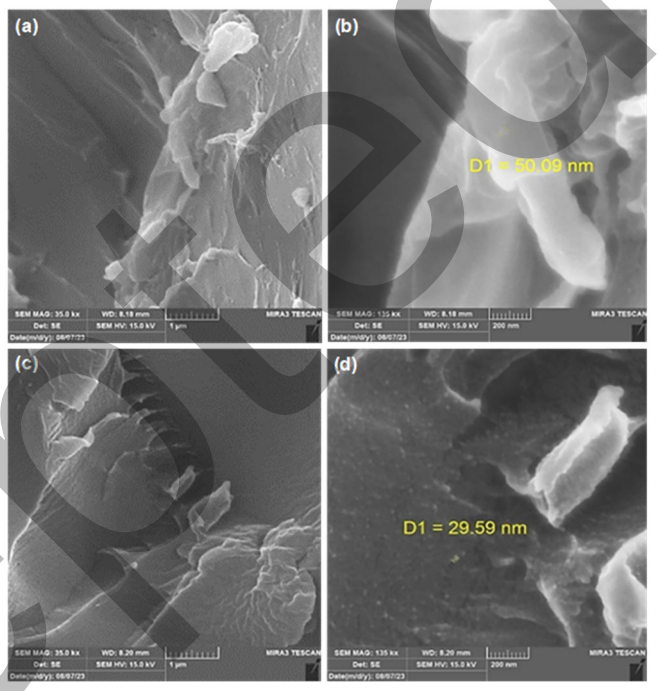

Fig 4. FESEM images of p(CS-co-AA)/MWCNTs (a,b) before and (c,d) after OFL loaded

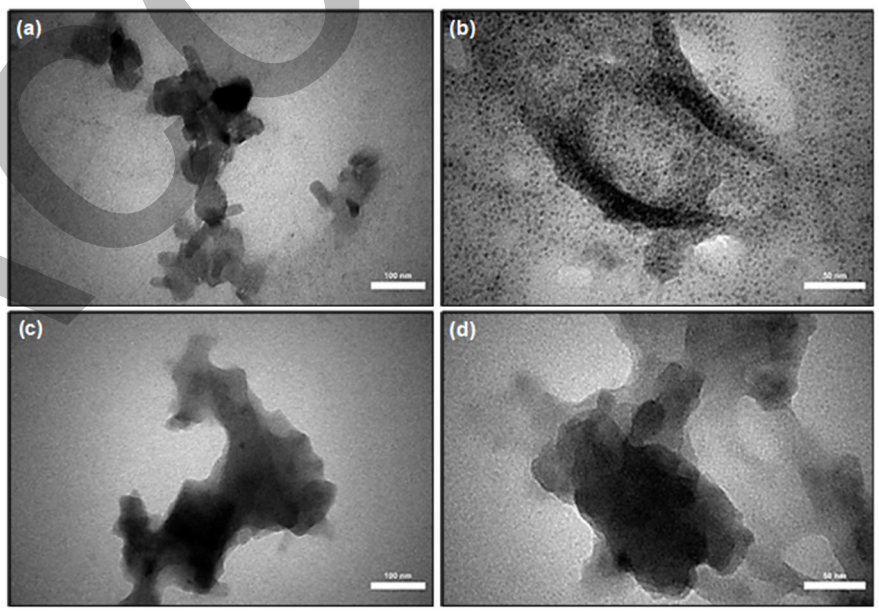

Fig 5. TEM images of p(CS-co-AA)/MWCNTs (a,b) before and (c,d) after OFL loaded

volume, which also provided evidence for the surface's amorphous character.

The thermal degradation of the p(CS-co-AA)/MWCNTs and OFL composites has been studied by TGA/DTG, which monitors the sample's mass change over a temperature range of 0–800 °C at a heating rate of 20 °C/min. Fig. 6(a) demonstrates the thermal stability of the composite material, indicating that it remains intact without any structural damage within the temperature range of 0–95 °C. The TGA graph showed a loss of 4.44% between 75–178 °C, which was assigned to water loss. The DTG curve shows a significant loss centered at 279 °C. This mass loss (27.91%) was due to the decomposition of the COOH, OH, and COC groups in the form of CO_2 and CO [40]. Another significant major weight loss (52.38%) between 317–523 °C, which can be attributed to the degradation of the residual organic moieties that are attached to the carbon substrate. The high temperature (> 270 °C) needed to decompose the organo–carbon material clearly indicated that p(CS-co-AA) had been chemically grafted on CNTs. TGA of OFL Composite in Fig. 6(b) observed three exothermic transformations centered at 144, 254, and 414 °C. The first exothermic transformation can be ascribed to the loss of adsorbed water, whereas the second and third changes are attributed to the structure of the polymer and adsorbed drug.

Fig. 7(a) displays the nitrogen adsorption isotherm determined for p(CS-co-AA)/MWCNTs. The pore size distribution is depicted in the inset graph. Capillary condensation, is marked by the appearance of the hysteresis loop, which is between 0.4 and 1.0 p/p_0. This is evidence of the existence of mesoporous pores in the composite. The adsorption-desorption isotherm of OFL Composite is presented in Fig. 7(b) (inset is pore size graph). The hysteresis loop for OFL was found to close near zero relative pressure. The ofloxacin immobilization produced a surface-modified material with a low surface area and a mesoporous structure.

The BET surface area of p(CS-co-AA)/MWCNTs was found to be 16.40 m^2/g and an average pore diameter of 5.08 nm (BJH model). The surface area and average pore diameter of OFL were reported to be 11.20 m^2/g and 4.95 nm, respectively. Compared to p(CS-co-AA)/MWCNTs, the pore size and surface area of OFL were lower, including the drug within the composite matrix, which was likely responsible for this result. Table 1 shows the result of BET and EDX analysis.

Fig. 8 shows that the nanocomposite of p(CS-co-AA)/MWCNTs, both unloaded and loaded with OFL, has zeta potential values of −46.5 and −68.4 mV, respectively. This indicates that the nanocomposite is highly anionic. The negative charge magnitude is important in binding to the positively charged surface of the cell membrane. One potential explanation for the observed heightened stability and augmented retinal permeability may be attributed to this factor [41].

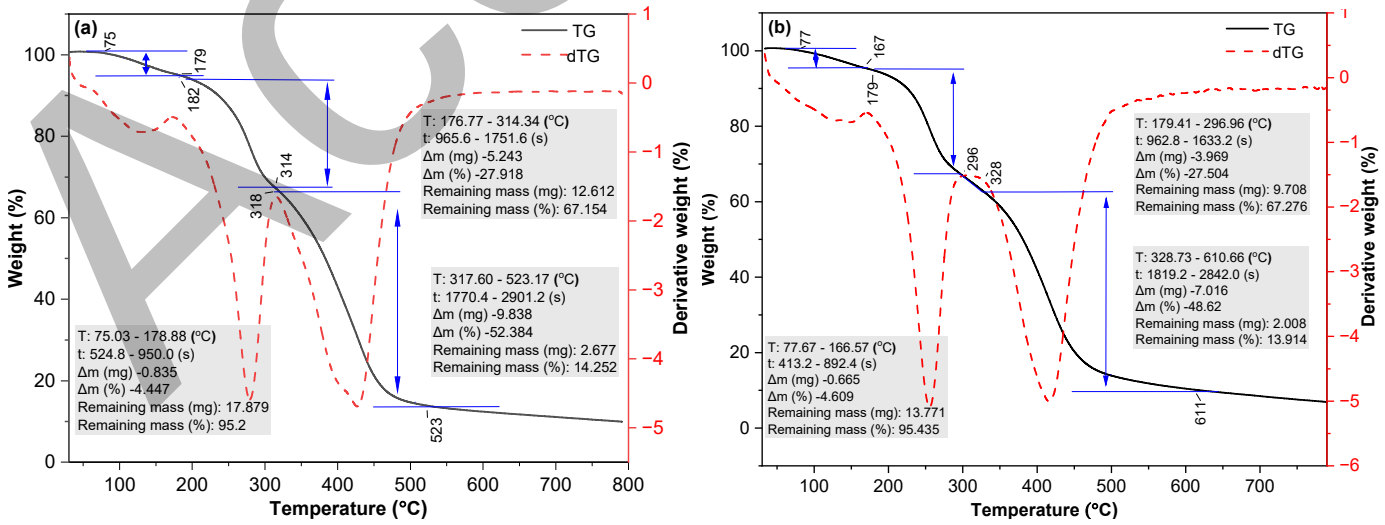

Fig 6. TGA and DTA thermograms of p(CS-co-AA)/MWCNTs (a) before (a) and (b) after loaded OFL

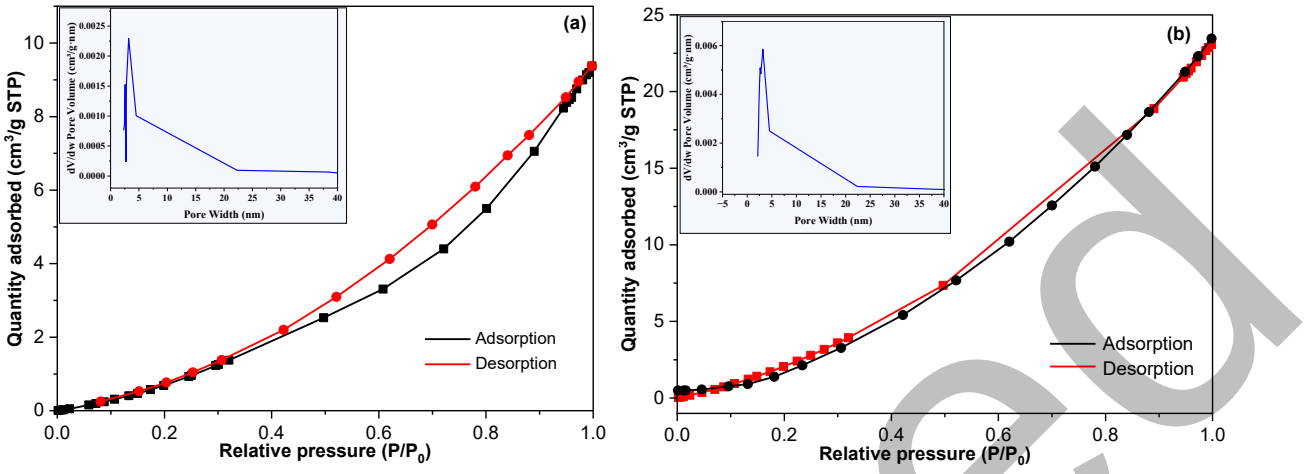

Fig 7. Nitrogen adsorption isotherms (inset pore size distribution) for the p(CS-co-AA)/MWCNTs (a) before and (b) after loading of OFL

Table 1. The BET and elemental analysis for p(CS-co-AA)/MWCNTs and OFL-p(CS-co-AA)/MWCNTs

Sample	Elemental analysis (%)			Surface area	Average pore	Average pore
	C	O	F	(m^2/g)	volume (cm^3/g)	diameter (nm)
p(CS-co-AA)/MWCNTs	56.150	43.850	0.000	16.440	0.020	5.080
OFL- p(CS-co-AA)/MWCNTs	56.700	43.110	0.190	11.270	0.053	4.950

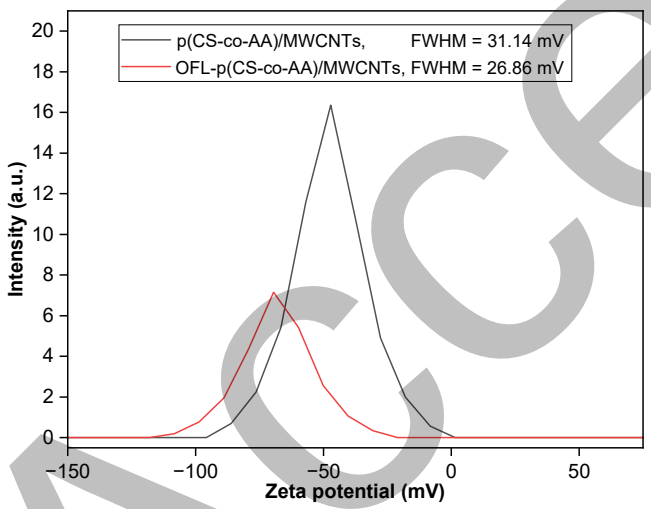

Fig 8. Zeta potential distribution of the p(CS-co-AA)/MWCNTs before and after OFL loaded

The understanding of negative zeta potential values is well-established in academic literature. In the case of untreated powders, the surface of CS and acrylic acid is found to be enveloped by oxygen-containing functional groups, mainly COOH and C=O, which are formed during the preparation of nanocomposites. The negative zeta potential in the nanocomposite surface can be attributed to carboxyl and carbonyl groups dissociation [42].

Swelling Study

The investigation focused on the swelling rates of p(CS-co-AA)/MWCNTs at different pH levels (2–10) within the temperature of 25 °C. The data presented in Fig. 9 demonstrates that the rate of swelling exhibits a rapid early increase, followed by a gradual decrease until it eventually reaches a condition of equilibrium. The swelling rate for p(CS-co-AA)/MWCNTs is rapid, initially increasing within the first 5 h and slowing down until it reaches a stable state after approximately 12 h. The maximum swelling percentage is observed in alkaline conditions, reaching 861% when the pH 10, due to the amino groups of CS almost existing in the form of $-NH_2$ under the strong alkaline conditions, where the protonation effect could be neglected. All of the carboxyl (–COOH) groups underwent ionization to form carboxylate ($-COO^-$) ions, and the repulsion between molecular chains continued to intensify as the number of carboxyl groups in the nanocomposite increased. The molecular chain noted significant elongation, substantially improving water absorption capacity [43]. The pKa value of the carboxyl group on acrylic acid (AA) is approximately 4.1 at a pH of 2, while the pKa value of

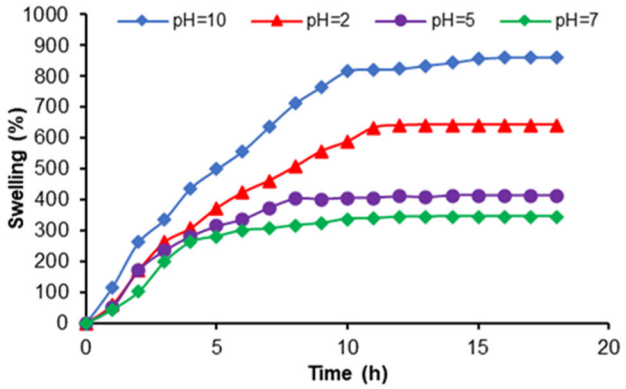

Fig 9. Time dependence of swelling values of p(CS-co-AA)/MWCNTs nanocomposite

the amino group ($-NH_3^+$) on CS is around 6.5 [44-45]. The increase in size of the nanocomposite was ascribed to the presence of protonated amines in acidic conditions when AA was not charged. As a result, the swelling ratio reached 642%. The electrostatic repulsion between charges resulted in the relaxing of the macromolecular chain. Simultaneously, the attraction between $-NH_3^+$ and water molecules also had a notable impact, promoting the absorption of greater quantities of water [43].

The nanocomposite exhibited a reduced swelling ratio at pH levels of 5 and 7. The dissociation of AA (where CS was non-charged) led to a higher swelling ratio at pH 7 compared to pH 2. At pH 7, most of the –COOH groups existed as $-COO^-$ ions, resulting in strong electrostatic repulsion between these ions. This improved the nanocomposite's water absorption capacity. In addition, the –COOH, $-NH_2$, and –OH groups formed hydrogen bonds that caused the polymer chain to contract, leading to a reduction in its overall swelling capacity.

Water Evaporation Rate

Hydrogen bonds forming between water and the hydrogel prevent water evaporation. The percentage of loss of water molecules every 1 h interval at room temperature was 50 to 72% of nanocomposite (Fig. 10). As time progressed, the evaporation rate increased significantly. All nanocomposites retained a percentage of 29–40% of the original water after 25 h. The p(CS-co-AA)/MWCNTs display a high capacity for preserving moisture. The number of hydrophilic groups (COOH and $CONH_2$) per unit volume of the hydrogel correlates with the number of bound water molecules in the swollen nanocomposite. On the other hand, when polymerization occurs, the resulting nanocomposites have a heterogeneous network structure that allows for greater water absorption and numerous connective pathways via which water can diffuse out [46].

Drug Loading Efficiency and Release

Drug release from the nanocomposite was examined in triplicate at different pH levels. OFL drug loading achieved a peak efficiency of 86%. Fig. 11 depicts the graphical representation of the drug release behavior from the nanocomposite. The plot illustrates the cumulative percentage of drug release, averaged from three replicates, vs. time (h). Studies of release were

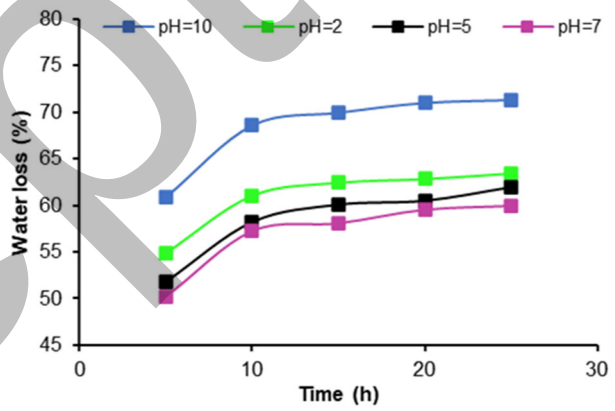

Fig 10. Percentage of water loss for the p(CS-co-AA)/MWCNTs

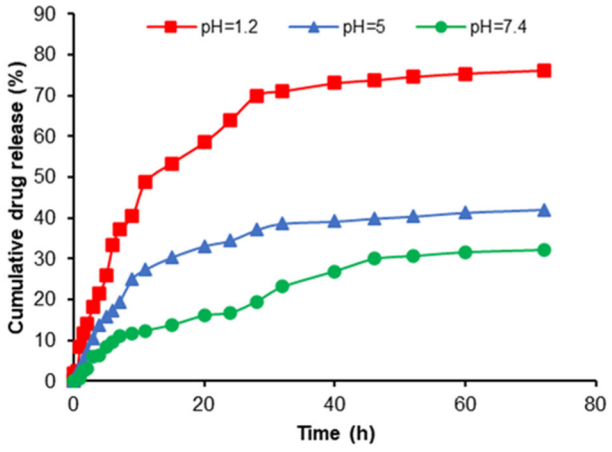

Fig 11. *In-vitro* release of OFL from OFL-loaded p(CS-co-AA)/MWCNTs nanocomposites at different pH conditions

conducted for 72 h at varying pH levels. The first "burst" effect of the drug was due to a swelling of the sample membrane caused by the drug diffusion. Due to the porous nature of the p(CS-co-AA)/MWCNTs nanocomposite, the drug at the sample's surface was released at a considerably higher rate than the drug contained deeper inside the nanocomposite [47].

It was observed that the release of the OFL drug from the nanocomposite was higher in pH 1.2 compared to pH 5 and 7.4, which is consistent with the results of the swelling process. The OFL drug has a low solubility in the neutral pH range. Therefore, the release results indicate that the amount of swelling of the nanocomposite controls the release of the drug compared to the dissolution process, where a high swelling ratio for nanocomposite leads to an increase in the size of the pores within the nanocomposite. Therefore, it is easy to see from the diffusion process of the OFL drug from the larger pore size, observed in pH = 1.2, that the amount of OFL released from the nanocomposite was estimated at 76% at 72 h. The drug release% at pH = 5 and pH = 7.4 were 42 and 32%, respectively; the decrease in drug release was due to the sharp decrease in the ability of the nanocomposite to swell.

On the other hand, the nanocomposite has a negative surface charge, as proved in zeta potential analysis, which resulted in an enhanced electrostatic attraction under natural conditions. The electrostatic interaction between protonated OFL and the nanocomposite surface is reduced in acidic conditions relative to that observed with a higher negative surface charge [48]. These results indicate that this system is an ideal and preventive method for delivering OFL and increasing the efficiency of the drug.

■ CONCLUSION

In this study, p(CS-co-AA)/MWCNTs nanocomposite were prepared using free radical polymerization for adsorption of the OFL and drug delivery. The findings indicated that the maximum drug-loading rate of OFL was 86%. Moreover, the pH sensitivity of the p(CS-co-AA)/MWCNTs composite facilitated the substantial release of a significant quantity of medication in aqueous buffered solution at a pH of 1.2. The average rate of drug release was measured to be 76.0% after a 72 h duration. On the other hand, the release of the drug at pH 5.0 and pH 7.4 was 42.0 and 32.0%, respectively. The maximum drug release was observed in an acidic medium. Therefore, the proposed p(CS-co-AA)/MWCNTs nanocomposite is a container to transfer the OFL drug to the target medium without side effects.

■ ACKNOWLEDGMENTS

The authors express their gratitude to the Department of Chemistry at the College of Science, Al-Qadisiyah University, for their generous provision and unwavering support.

■ CONFLICT OF INTEREST

All the authors have declared that there is no conflict of interest.

■ AUTHOR CONTRIBUTIONS

The idea was conceived by Zeina Mohammad Kadam. Zainab Jasim Khudair conducted the experiment, calculated, wrote and revised the manuscript. All authors agreed to the final version of this manuscript.

■ REFERENCES

[1] Basher, N.A., and Ali, A.A., 2022, Hydrothermal Synthesis and application of nanocomposite as a demulsifier in crude oil processing, *Egypt. J. Chem.*, 65 (6), 741–752.

[2] Sahu, M.K., Yadav, R., and Tiwari, S.P., 2023, Recent advances in nanotechnology, *Int. J. Nanomater. Nanotechnol. Nanomed.*, 9 (1), 15–23.

[3] Panigrahi, B.K., and Nayak, A.K., 2020, Carbon nanotubes: An emerging drug delivery carrier in cancer therapeutics, *Curr. Drug Delivery*, 17 (7), 558–576.

[4] Mekuye, B., and Abera, B., 2023, Nanomaterials: An overview of synthesis, classification, characterization, and applications, *Nano Sel.*, 4 (8), 486–501.

[5] Baig, N., Kammakakam, I., and Falath, W., 2021, Nanomaterials: A review of synthesis methods,

properties, recent progress, and challenges, *Mater. Adv.*, 2 (6), 1821–1871.

[6] Mahor, A., Singh, P.P., Bharadwaj, P., Sharma, N., Yadav, S., Rosenholm, J.M., and Bansal, K.K., 2021, Carbon-based nanomaterials for delivery of biologicals and therapeutics: A cutting-edge technology, *C*, 7 (1), 19.

[7] Subagio, A., Prihastanti, E., and Ngadiwiyana, N., 2020, Application of functionalized multi-walled carbon nanotubes for growth enhancement of mustard seed germination, *Indones. J. Chem.*, 20 (1), 120–129.

[8] Yudianti, R., Hutabarat, L.G., Irmawati, Y., Widodo, H., Indayaningsih, N., and Magfirah, A., 2020, Carbon nanotube network as an electron pathway in nanocomposite films, *Int. J. Mater. Res.*, 111 (3), 197–203.

[9] Lavagna, L., Nisticò, R., Musso, S., and Pavese, M., 2021, Functionalization as a way to enhance dispersion of carbon nanotubes in matrices: A review, *Mater. Today Chem.*, 20, 100477.

[10] Wu, Y., Zhao, X., Shang, Y., Chang, S., Dai, L., and Cao, A., 2021, Application-driven carbon nanotube functional materials, *ACS Nano*, 15 (5), 7946–7974.

[11] Rathinavel, S., Priyadharshini, K., and Panda, D., 2021, A review on carbon nanotube: An overview of synthesis, properties, functionalization, characterization, and the application, *Mater. Sci. Eng., B*, 268, 115095.

[12] Singhai, N.J., and Ramteke, S., 2020, Functionalized carbon nanotubes: Emerging applications in the diverse biomedical arena, *Curr. Nanosci.*, 16 (2), 170–186.

[13] Aslam, M.M.A., Kuo, H.W., Den, W., Usman, M., Sultan, M., and Ashraf, H., 2021, Functionalized carbon nanotubes (CNTs) for water and wastewater treatment: Preparation to application, *Sustainability*, 13 (10), 5717.

[14] Chio, L., Pinals, R.L., Murali, A., Goh, N.S., and Landry, M.P., 2020, Covalent surface modification effects on single-walled carbon nanotubes for targeted sensing and optical imaging, *Adv. Funct. Mater.*, 30 (17), 1910556.

[15] Jha, R., Singh, A., Sharma, P.K., and Fuloria, N.K., 2020, Smart carbon nanotubes for drug delivery system: A comprehensive study, *J. Drug Delivery Sci. Technol.*, 58, 101811.

[16] Dubey, R., Dutta, D., Sarkar, A., and Chattopadhyay, P., 2021, Functionalized carbon nanotubes: Synthesis, properties and applications in water purification, drug delivery, and material and biomedical sciences, *Nanoscale Adv.*, 3 (20), 5722–5744.

[17] Sonowal, L., and Gautam, S., 2024, Advancements and challenges in carbon nanotube-based drug delivery systems, *Nano-Struct. Nano-Objects*, 38, 101117.

[18] Debnath, S.K., and Srivastava, R., 2021, Drug delivery with carbon-based nanomaterials as versatile nanocarriers: Progress and prospects, *Front. Nanotechnol.*, 3, 644564.

[19] Das, S.S., Bharadwaj, P., Bilal, M., Barani, M., Rahdar, A., Taboada, P., Bungau, S., and Kyzas, G.Z., 2020, Stimuli-responsive polymeric nanocarriers for drug delivery, imaging, and theragnosis, *Polymers*, 12 (6), 1397.

[20] Bai, L., Li, X., He, L., Zheng, Y., Lu, H., Li, J., Zhong, L., Tong, R., Jiang, Z., Shi, J., and Li, J., 2019, Antidiabetic potential of flavonoids from traditional Chinese medicine: A review, *Am. J. Chin. Med.*, 47 (05), 933–957.

[21] Sharma, P., and Scott, D.G.I., 2015, Optimizing methotrexate treatment in rheumatoid arthritis: The case for subcutaneous methotrexate prior to biologics, *Drugs*, 75 (17), 1953–1956.

[22] Kurban, M., and Muz, İ., 2020, Theoretical investigation of the adsorption behaviors of fluorouracil as an anticancer drug on pristine and B-, Al-, Ga-doped C36 nanotube, *J. Mol. Liq.*, 309, 113209.

[23] Khezri, B., Beladi Mousavi, S.M., Krejčová, L., Heger, Z., Sofer, Z., and Pumera, M., 2019, Ultrafast electrochemical trigger drug delivery mechanism for nanographene micromachines, *Adv. Funct. Mater.*, 29 (4), 1806696.

[24] Campuzano, S., Esteban-Fernández de Ávila, B., Yáñez-Sedeño, P., Pingarrón, J.M., and Wang, J., 2017, Nano/microvehicles for efficient delivery and (bio)sensing at the cellular level, *Chem. Sci.*, 8 (10), 6750–6763.

[25] Raj, H., Sharma, S., Sharma, A., Verma, K.K., and Chaudhary, A., 2021, A novel drug delivery system: Review on microspheres, *J. Drug Delivery Ther.*, 11(2-S), 156–161.

[26] Kompella, U.B., Hartman, R.R., and Patil, M.A., 2021, Extraocular, periocular, and intraocular routes for sustained drug delivery for glaucoma, *Prog. Retinal Eye Res.*, 82, 100901.

[27] Moiseev, R.V., Morrison, P.W.J., Steele, F., and Khutoryanskiy, V.V., 2019, Penetration enhancers in ocular drug delivery, *Pharmaceutics*, 11 (7), 321.

[28] Rashki, S., Asgarpour, K., Tarrahimofrad, H., Hashemipour, M., Ebrahimi, M.S., Fathizadeh, H., Khorshidi, A., Khan, H., Marzhoseyni, Z., Salavati-Niasari, M., and Mirzaei, H., 2021, Chitosan-based nanoparticles against bacterial infections, *Carbohydr. Polym.*, 251, 117108.

[29] Rusu, A., Munteanu, A.C., Arbănași, E.M., and Uivarosi, V., 2023, Overview of side-effects of antibacterial fluoroquinolones: New drugs versus old drugs, a step forward in the safety profile?, *Pharmaceutics*, 15 (3), 804.

[30] Khudair, Z.J., and Kadam, Z.M., 2024, Adsorption behavior of chitosan-MWCNTS nanocomposite for the elimination of ofloxacin medication, *Chem. J. Mold.*, 19 (1), 84–92.

[31] Wang, Z., Ning, A., Xie, P., Gao, G., Xie, L., Li, X., and Song, A., 2017, Synthesis and swelling behaviors of carboxymethyl cellulose-based superabsorbent resin hybridized with graphene oxide, *Carbohydr. Polym.*, 157, 48–56.

[32] Enayatpour, B., Rajabi, M., Yari, M., Reza Mirkhan, S.M., Najafi, F., Moradi, O., Bharti, A.K., Agarwal, S., and Gupta, V.K., 2017, Adsorption/desorption study of proteins onto multi-walled carbon nanotubes and amino multi-walled carbon nanotubes surfaces as adsorbents, *J. Mol. Liq.*, 231, 566–571.

[33] Pourjavadi, A., Hosseinzadeh, H., and Sadeghi, M., 2007, Synthesis, characterization and swelling behavior of gelatin-g-poly(sodium acrylate)/kaolin superabsorbent hydrogel composites, *J. Compos. Mater.*, 41 (17), 2057–2069.

[34] Witono, J.R., Noordergraaf, I.W., Heeres, H.J., and Janssen, L.P.B.M., 2014, Water absorption, retention and the swelling characteristics of cassava starch grafted with polyacrylic acid, *Carbohydr. Polym.*, 103, 325–332.

[35] Chang, L., Xu, L., Liu, Y., and Qiu, D., 2021, Superabsorbent polymers used for agricultural water retention, *Polym. Test.*, 94, 107021.

[36] Pathania, D., Gupta, D., Kothiyal, N.C., Sharma, G., Eldesoky, G.E., and Naushad, M., 2016, Preparation of a novel chitosan-g-poly(acrylamide)/Zn nanocomposite hydrogel and its applications for controlled drug delivery of ofloxacin, *Int. J. Biol. Macromol.*, 84, 340–348.

[37] Shi, Q., Anishiya Chella Daisy, E.R., Yang, G., Zhang, J., Mickymaray, S., Alfaiz, F.A., Paramasivam, A., and Rajan, M., 2021, Multifeatured guar gum armed drug delivery system for the delivery of ofloxacin drug to treat ophthalmic dieases, *Arabian J. Chem.*, 14 (5), 103118.

[38] Kaya, D., Küçükada, K., and Alemdar, N., 2019, Modeling the drug release from reduced graphene oxide-reinforced hyaluronic acid/gelatin/poly(ethylene oxide) polymeric films, *Carbohydr. Polym.*, 215, 189–197.

[39] Liu, Q., Xu, K., Hu, G., Zeng, F., Li, X., Li, C., and Zhang, Y., 2022, Underwater superelastic MOF/polyacrylamide/chitosan composite aerogel for efficient 2,4-dichlorophenoxyacetic acid adsorption, *Colloids Surf., A*, 635, 127970.

[40] Yang, H., Yan, R., Chen, H., Lee, D.H., and Zheng, C., 2007, Characteristics of hemicellulose, cellulose and lignin pyrolysis, *Fuel*, 86 (12-13), 1781–1788.

[41] Long, Y.M., Zhao, X.C., Clermont, A.C., Zhou, Q.F., Liu, Q., Feener, E.P., Yan, B., and Jiang, G.B., 2016, Negatively charged silver nanoparticles cause retinal vascular permeability by activating plasma

contact system and disrupting adherens junction, *Nanotoxicology*, 10 (4), 501–511.

[42] Ginés, L., Mandal, S., Ahmed, A.I., Cheng, C.L., Sow, M., and Williams, O.A., 2017, Positive zeta potential of nanodiamonds, *Nanoscale*, 9 (34), 12549–12555.

[43] Rohindra, D.R., Nand, A.V., and Khurma, J.R., 2004, Swelling properties of chitosan hydrogels, *South Pac. J. Nat. Appl. Sci.*, 22 (1), 32–35.

[44] Yang, J., Dahlström, C., Edlund, H., Lindman, B., and Norgren, M., 2019, pH-responsive cellulose–chitosan nanocomposite films with slow release of chitosan, *Cellulose*, 26 (6), 3763–3776.

[45] Zargar, V., Asghari, M., and Dashti, A., 2015, A review on chitin and chitosan polymers: Structure, chemistry, solubility, derivatives, and applications, *ChemBioEng Rev.*, 2 (3), 204–226.

[46] Liu, H., Liu, M., Zhang, L., Ma, L., Chen, J., and Wang, Y., 2010, Dual-stimuli sensitive composites based on multi-walled carbon nanotubes and poly(*N*,*N*-diethylacrylamide-co-acrylic acid) hydrogels, *React. Funct. Polym.*, 70 (5), 294–300.

[47] Sharma, S., Kaur, J., Sharma, G., Thakur, K.K., Chauhan, G.S., and Chauhan, K., 2013, Preparation and characterization of pH-responsive guar gum microspheres, *Int. J. Biol. Macromol.*, 62, 636–641.

[48] Lestari, W.A., Wahyuningsih, S., Gomez-Ruiz, S., and Wibowo, F.R., 2022, Drug loading ability and release study of various size small mesoporous silica nanoparticle as drug carrier, *J. Phys.: Conf. Ser.*, 2190 (1), 012032.